Sample-in-the-Loop Laser Speckle Contrast Imaging Based on Optimization

Máté Siket[1,2], Imre Jánoki[1], Ádám Nagy[1], and Péter Földesy[1]

[1]Institute for Computer Science and Control, Kende utca 13-17, H-1111, Budapest, Hungary; siket.mate@sztaki.hu; janoki.imre.gergely@sztaki.hu; nagy.adam@sztaki.hu; foldesy.peter@sztaki.mta.hu
[2]Physiological Controls Research Center, Óbuda University, Bécsi út 96/b, Budapest, H-1034

Abstract: Laser Speckle Contrast Imaging (LSCI) is an optical method mainly used for creating blood flow maps. Despite its beneficial properties, the technique is yet to find a place in clinical practice. In this work, we propose a setup for LSCI to overcome some of the disadvantages associated with the method. We call the setup the sample-in-the-loop LSCI as it is based on the feedback of the captured image, which is determined by the properties of the sample and the experimental setup. We investigate and demonstrate the method in three exemplary scenarios: optimization to specific contrast setpoint, sensitivity maximization and dynamic range maximization. These goals are achieved by using optimization on the laser light pulse sequence and on the exposure time of the digital camera.

Keywords: laser speckle contrast imaging; sample-in-the-loop; time varied illumination; dynamic range maximization

1 Introduction

Despite recent years show a decrease or slowed growth in the utilization rates of non-invasive diagnostic imaging modalities, they are still cornerstones in terms of clinical applications and are the main focus of scientific research [1]. The medical imaging practice has its traditional, proven, widely applied techniques such as X-ray, computed tomography, magnetic resonance imaging, or ultrasound. However, there are modalities yet to become a part of clinical practice, one of which is Laser Speckle Contrast Imaging (LSCI) [2, 3]. A possible drawback of LSCI is the sensitivity to calibration, dynamic range, and exposure [4, 5]. In our current work, we propose a way to alleviate these by partly automating processes based on feedback. LSCI utilizes the interference pattern caused by the reflection of coherent light from a medium with static and dynamic scatterers [6]. In the specific case when the reflective medium is completely static, the imaging device observes a frozen pattern of the so-called speckles. However, if motion occurs (e.g. blood flows) the pattern changes and

decorrelates in time. The level of decorrelation can be quantified by calculating the contrast in a region of interest (ROI). Carrying out the calculation using a sliding window results in a contrast map, which tells us about the relative flow speeds in vessels with various sizes, the progression of diabetes-induced vascular complications [7] or regeneration of a burned tissue [8, 9]. Among others, one of the disadvantages of the technique is the relatively low dynamic range. Previously multi-exposure techniques have been investigated to increase the dynamic range and to suppress the detrimental effect of static scatterers [10–12]. Furthermore, under- or overexposure can also greatly affect the observed contrast values. To this end, [13] introduced a correction term to counteract the effect of underexposed images. [14] recommends adjusting the average intensity in the image to be around or slightly below the middle of the dynamic range of the sensor.

A recent study [15] showed that the dynamic range of LSCI can be greatly improved by utilizing a novel, time-varied illumination during camera exposure. Discrete pulsetrains were used for the realization of the time-varied illumination. Different shapings of the discrete pulsetrains have been investigated, however, they share the common aspect of predefinition or model-based optimization of the sequence, and both are done offline. The offline approach is disadvantageous because (i) it requires an accurate model, (ii) two measurements are needed (before and after identification of the model), and (iii) the sample is subject to changes between measurements.

The experienced drawbacks motivated the creation of an alternative method. Here, we propose to optimize the discrete pulse sequence in an online, model-free manner, calling it the sample-in-the-loop approach. Although the concept originates from the time-varied illumination approach we do not limit ourselves to that specific case. In contrast to the varied illumination, hereinafter, we refer to the constant illumination as the continuous wave operation of the laser light. Compared to multiexposure methods [11, 12, 16], the online, optimization-based approach can take into account the average intensity; instead of making post-measurement corrections [13, 17] can keep the intensity in a favorable range. Also, the method does not need an extensive calibration process, as it was proposed in [18].

We demonstrate the concept in a custom-developed channel slide through three experimental scenarios: optimization to specific contrast setpoint, sensitivity maximization, and dynamic range maximization. The three distinct scenarios touch on different aspects; continuous wave versus time-varied operation dictates the usage of different optimization algorithms and scenarios can differ in the number of required ROIs.

The paper is structured as follows. First, in Section 2 we detail the sample in the loop setup with the designed channel slide. Next, the approach to the laser pulse optimization is given, defining the optimization goals and methods. In the Results section, the three experimental scenarios are investigated separately, and finally, in Section 4.3 conclusions are drawn.

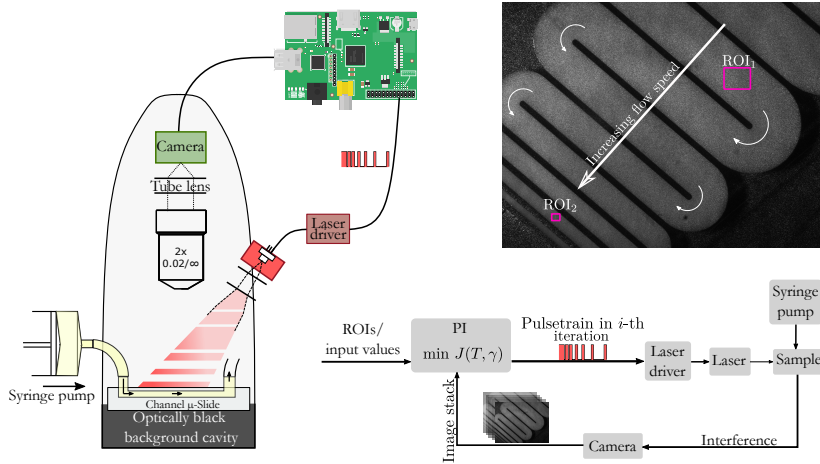## 2   Sample in the loop setup

Figure 1

The experimental setup can be seen on the left-hand side. A medical syringe pump provides a constant flow speed, while the laser and the digital camera are controlled by the Raspberry Pi. A raw speckle image with a typical ROI selection is illustrated in the upper right corner. The schematic diagram in the lower right corner summarizes the sample-in-the-loop LSCI method.

A Raspberry Pi 4 Model B carries out the digital pulse wave generation, the camera control, and the image processing tasks through a custom-developed software. Fig. 1 depicts the sample-in-the-loop experimental setup. The protocol of an experiment can be summarized as follows: First, the user selects the optimization scenario and the related thresholds and reference values. Second, an initial pulse wave is generated to capture a single image for ROI selection purposes. Afterward, the optimization algorithm updates the pulse sequences based on 10 averaged contrast images (with a resolution of 2000x1500 pixels). It continues to do so until a maximum number of iterations or termination limit is reached. The pulsetrains (leaving the GPIO pins of the Pi) control the 660 nm 50 mW laser diode through a laser driver (LDP-VRM 01-12 CA, PicoLAS, Germany) and at the same time trigger the monochrome digital camera (Basler acA2040-55um). Based on preliminary investigations we limited the minimum pulse width to 10 μs. With shorter pulses the proportion of laser transients becomes dominant, which introduces two unwanted effects: average intensity significantly lowers, and contrast lowers because of the larger proportion of incoherent light [19]. Furthermore, the laser is mounted in a thermally stabilized mount (LDM21, Thorlabs, Germany) driven by a Thorlabs TED200C temperature controller. The constant temperature improves contrast by reducing temperature-induced laser mode hopping.

2.1   Designed channel slide

For demonstration purposes, we designed a channel slide 2, where the cross sections range linearly from 100 μm to 1000 μm in 100 μm increments. We created a simulation of the flow in the channel design using COMSOL Multiphysics [20], which showed that the velocities at the center of the straight sections are roughly proportional to the diameter. The microfluidic channel slide was created using PDMS bonded to glass with a depth of 100 μm.
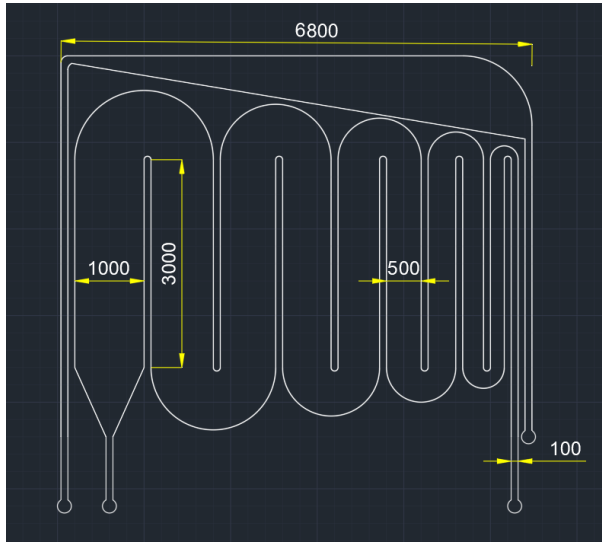

Figure 2
The channel slide design we used for evaluation. Based on the simulated model, the flow speeds at the center of each straight section is proportional to their diameter. The annotated sizes on the image are in μm.

3   Laser pulse optimization

The validity of pulsed speckle contrast imaging has already been proven in [21]. In this method, uniform intensity and uniform length discrete laser pulses with uniform pulse rates are used instead of continuous wave illumination. Instead of the well-known multi-exposure methods [11, 12] that were developed to extend the dynamic range, we use time-varied illumination laser speckle contrast imaging [15] which is based on pulsed speckle contrast imaging. It uses laser pulsetrains of uniform intensity and uniform length discrete pulses, however, it changes the density of the pulses that ultimately simulates a varying intensity during a single exposure. Using a pulse sequence made of multiple density pulsetrains (e.g. 3 pulsetrains of equal length with 75%, 50% and 25% duty cycles concatenated) enables high dynamic range flow rate imaging during this

single exposure.

We made this discrete pulse sequence to be a function of a single variable. This function limits the number of feasible sequences but helps with the optimization problem by introducing only one more variable besides the exposure length. The additional parameter affects the spacing – in a form of a power function – between two consecutive high states. The sequence starts with an initial high state. The next high state is defined by the number of low states (n_{LOW}) following the initial high state as:

$$n_{LOW}(i) = round(i^{\gamma}) - 1, \tag{1}$$

where the discrete sequence is loaded with binary values from $i = 0$ to $i = \frac{T}{10\,\mu s}$, T is the exposure length, $\gamma >= 0$ is the spacing factor. If $n_{LOW} \leq 0$ the next state will remain a high state. The continuous wave laser setup is a limiting case when $\gamma = 0$, typically we evaluated $0 \leq \gamma \leq 1.4$. Fig. 3 illustrates how the spacing factor affects the average ROI intensity for different exposure lengths.
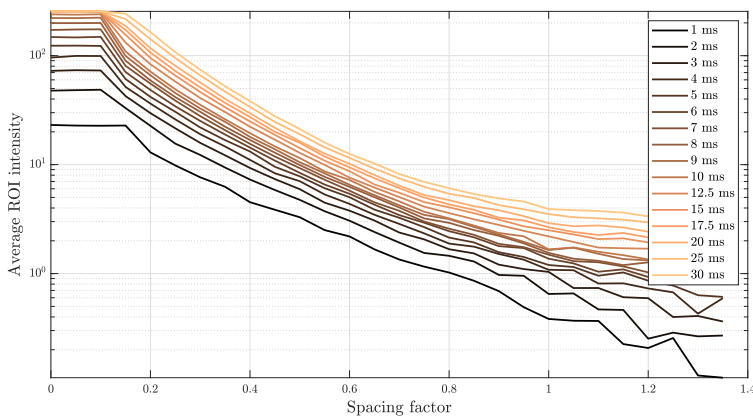

Figure 3

Measured average intensities in an ROI are visualized as a function of the spacing factor. It can be observed that after an initial interval between 0 and 0.1, a spacing factor of 1 reduces the intensity by more than an order of magnitude. Small values of the spacing factor would have only a visible effect on exposures above 30 ms.

The typical way of quantifying flow speed in LSCI is by means of contrast calculation. The speckle contrast is calculated on a single digital image or sequence of consecutive images (to descrease noise level), in both cases using a sliding window. The contrast is calculated by taking the quotient of the standard deviation and the mean of the intensities in the current window. The window size is usually $n \times n$, where n is in the range of 5 to 15 [22]. The spatial speckle

contrast is defined as:

$$\kappa = \frac{\sigma(I_s)}{\langle I_s \rangle},\tag{2}$$

where $\sigma(I_s)$ and $\langle I_s \rangle$ are the sample standard deviation and the sample mean in the current window. The choice of window size affects the noisiness and the resolution of the resulting contrast map. The contrast value is averaged on 10 consecutive images in order to reduce noise and improve the consistency of the optimization.

We defined three major optimization problems: contrast setpoint, sensitivity maximization, and dynamic range maximization. Previously it was shown in [13] that the intensity has a significant effect on the contrast values. Thus, besides the major objectives, all three share an optional penalization for underexposed images; a linear term penalizes the given parameter/parameter set when the average intensity falls below a predefined threshold in the ROIs. In our experimental setup ROI sizes ranged between 10x10 to 50x50 depending on the size of the evaluated cross-section in the channel slide.
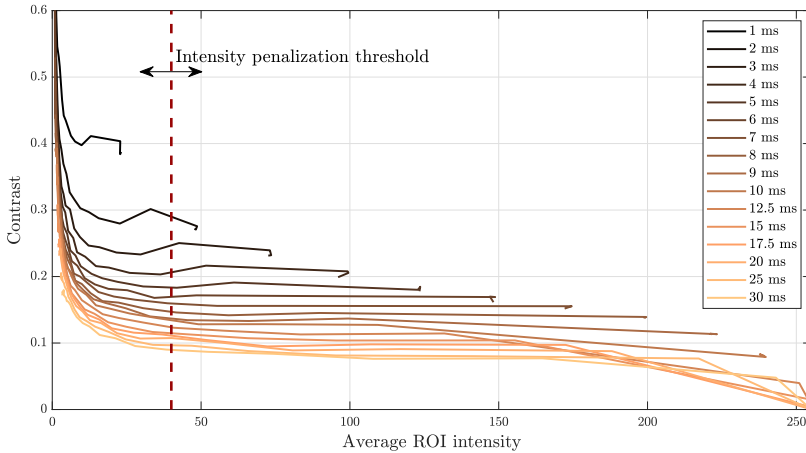

Figure 4

Observed speckle contrasts plotted with respect to the average ROI intensity. Low intensities can cause falsely observed large contrast values, while high intensities can cause falsely observed low contrast values. In order to avoid the potentially detrimental effects, a method of intensity penalization is implemented during the optimization. The figure indicates that a threshold around an intensity level of 40-50 guarantees a linear, flat response.

3.1   Contrast setpoint

Optimization based methods are widely used in control problems [23–26], we defined the first scenario as an optimization to setpoint contrast value. The user

can select an arbitrary ROI and define a desired average contrast value in that particular ROI. Then the gradient descent algorithm iteratively modifies the continuous wavelength, which also determines the exposure length of the camera. This first scenario aims to approach the sample-in-the-loop concept in the simplest manner. For this reason, we decided to optimize a single variable with the gradient descent method as follows:

$$T_{i+1} = T_i - \alpha \frac{\Delta J}{\Delta T},$$

(3)

where α is the step size, Δ denotes the differences in cost J and exposure length T between the i-th and $i-1$-th iteration.

$$
\begin{aligned}
\min_{T} \quad & J(T) = |\kappa(T) - \kappa_{ref}| + J_{exp.}, \\
\text{s.t.} \quad & T \in [1, 30], \\
& J_{exp.} = \begin{cases} 0, & \text{if} \quad \mu >= \mu_{ref}, \\ \frac{\mu - \mu_{ref}}{\lambda}, & \text{else.} \end{cases}
\end{aligned}
$$

(4)

where κ is the average calculated contrast in the ROI, κ_{ref} is the user-defined contrast setpoint, and μ_{ref} is the average intensity threshold. The offset from the reference intensity μ_{ref} is normalized by λ in order to scale the additional penalization in the range of the unpenalized cost, in our experimental setup, a reasonable value for the λ was around 40. The parameters of the control: α, the number of iterations, and the λ were determined based on multiple experiments with different channel slides and flow speeds.

3.2 Sensitivity maximization

The cost is defined as the inverse of the difference:

$$
\begin{aligned}
\min_{T} \quad & J(T) = \frac{1}{|\kappa_1(T) - \kappa_2(T)| + \varepsilon} + J_{exp.}, \\
\text{s.t.} \quad & T \in [1, 30], \\
& J_{exp.} = \begin{cases} 0, & \text{if} \quad \mu >= \mu_{ref}, \\ \frac{\mu - \mu_{ref}}{\lambda}, & \text{else.} \end{cases}
\end{aligned}
$$

(5)

where κ_1 and κ_2 are the average contrast values in the respective ROI and ε avoids division by zero.

3.3 Dynamic range maximization

Study [15] showed that by utilizing time variant illumination during the camera exposure the dynamic range of the laser speckle contrast imaging can be greatly improved.

$$\min_{T,\gamma} \quad J(T,\gamma) = |\kappa_1(T,\gamma) - \kappa_{ref}| + |\kappa_2(T,\gamma) - \kappa_{ref}| + J_{exp.},$$

$$\text{s.t.} \quad T \in [1,30], \quad \gamma \in [0,1.4], \tag{6}$$

$$J_{exp.} = \begin{cases} 0, & \text{if} \quad \mu >= \mu_{ref}, \\ \frac{\mu - \mu_{ref}}{\lambda}, & \text{else.} \end{cases},$$

where $\kappa_{ref.}$ is a user-defined contrast value, around which the sensitivity ought to be the least.

4   Results

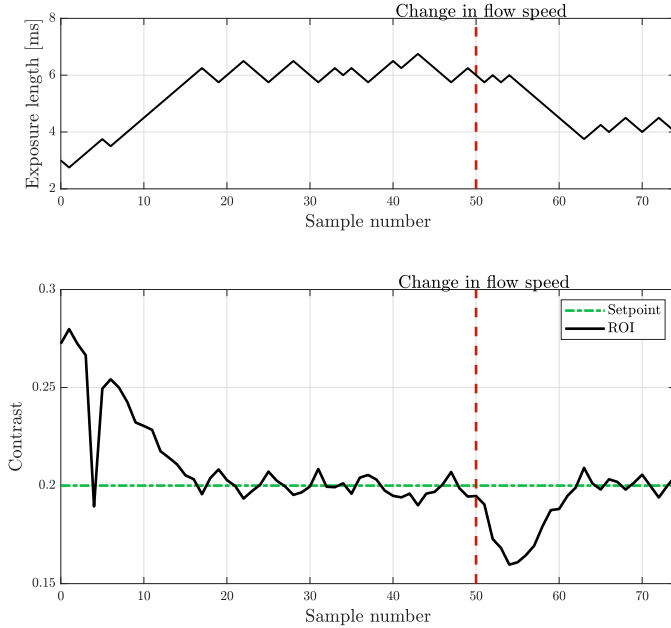## 4.1   Optimization to contrast setpoint

Figure 5

The set exposure length and measured contrast with respect to the current sample number are illustrated by solid black lines. The flow speed of the syringe pump has been modified during the experiment (denoted by the dashed red line), creating an external disturbance on the system. The contrast setpoint is depicted by the dashed green line.

Fig. 5 demonstrates the result of the first scenario, namely the optimization for a specific contrast value. A contrast value of 0.27 is observed with an initial exposure length of 3 ms. Then the gradient descent algorithm iteratively increases the exposure length to match the reference 0.2 contrast value. Besides the fluctuation caused by the measurement noises, the algorithm settles for an exposure length of 6 ms. When the disturbance occurs (in a form of flow speed change), the observed contrast drops by 0.05, but the algorithm compensates for it after a couple of iterations and settles for a new 4 ms exposure length. A change in flow speed induces a change in the measured contrast values, which are based on the captured image. The larger deviance in the contrast value ultimately results in a larger cost. A new optimum can be found by either increasing or reducing the exposure time so that deviance can be counteracted. The compensation can be done only in a feasible range of the parameters which determine the operation of the laser and the camera.

4.2　Sensitivity maximization

Despite that the optimization of the exposure length would be sufficient for sensitivity maximization, we carried out an experiment using both of the variables for demonstration purposes: the spacing factor and the exposure length.

Fig. 6 demonstrates well that the optimizer achieved the lowest costs when the spacing factor was close to zero. The small spacing factor in practical perspective translates to a continuous wave-like operation, which is otherwise expected to yield the best result in terms of sensitivity.
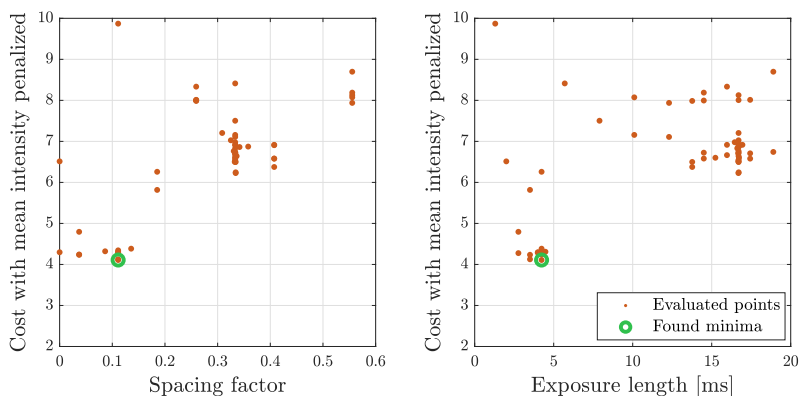

Figure 6
Evaluated spacing factor-exposure length combinations are illustrated during the sensitivity maximization scenario. It can be seen that the lowest costs are achieved if the optimizer converges the pulse sequence to the continuous wave operation.

4.3   Dynamic range maximization

In Fig. 7 we showcase an exemplary optimization using the grid search algorithm [27]. The algorithm aims to minimize the cost function given in (6). It can be seen that it converges to a spacing factor of around 0.3 and to an exposure length of 8 ms, where a minimum is found. In this multivariate scenario, the grid search algorithm was preferred in order to avoid the possibility of quick convergence to a local minimum.
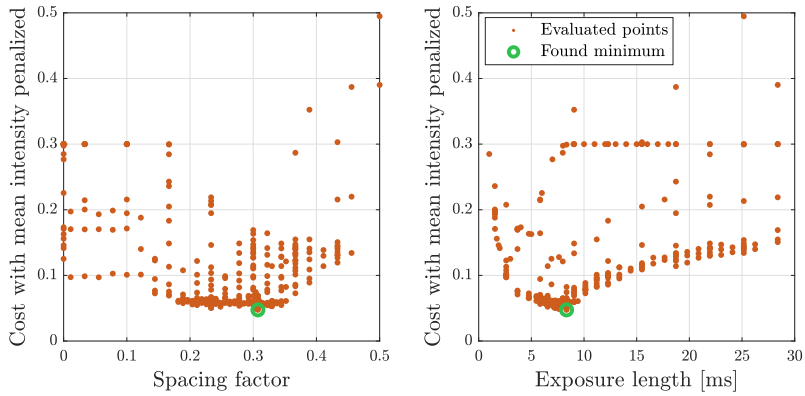

Figure 7

Evaluated spacing factor-exposure length combinations are illustrated during the dynamic range maximization scenario. It can be seen that the cost can be lowered by applying time-varying illumination. An optimal solution is found around a spacing factor of 0.3 and an exposure length of 8 ms.

We explored the effect of the spacing factor and exposure length in order to ascertain the cost surface and that the algorithm indeed found a minimum. The exposure length is varied in a range from 1 ms to 30 ms and the spacing factor is from 0 to 1.4. Fig. 8 and 9 depict the optimization surfaces given two different reference contrast values. The reference value of (6) is set to 0.1 in Fig. 8 and 0.3 in Fig. 9.
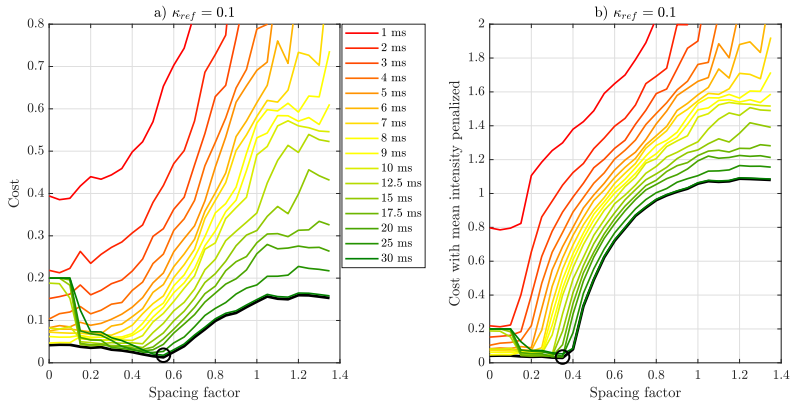
Figure 8
The measured optimization surface when the reference value is set to 0.1 is approximated with a family of curves. Subplot a) represents the "raw" cost, while subplot b) the cost when the average intensity is penalized.
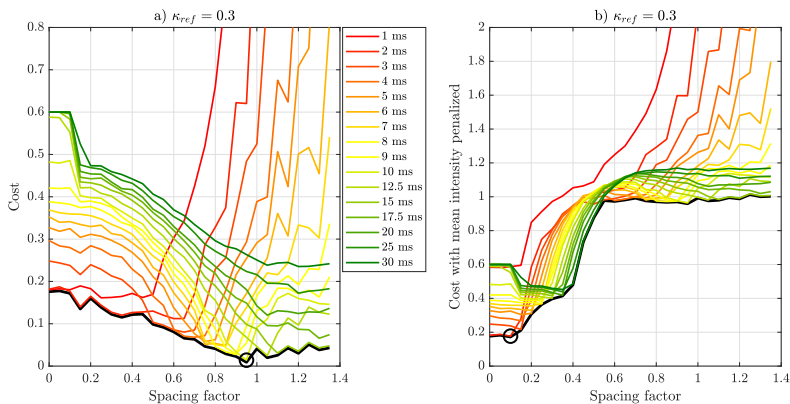

Figure 9
The measured optimization surface when the reference value is set to 0.3 is approximated with a family of curves. Subplot a) represents the "raw" cost, while subplot b) the cost when the average intensity is penalized.

The behavior of the cost function towards the minimum (0) and maximum (1.4) of the spacing factor is dominated by the phenomenon related to the average intensities. Firstly, for small values of the spacing factor, the laser switches to continuous wave-like operation, which means increased exposure. The increased exposure (mostly in the case of longer exposure times) leads to saturation, which in return lowers the observed contrast (as indicated in Fig. 4). Zero contrast values consequently saturate the cost function, as it can be seen in Fig. 8 and 9 subplots a) for exposure times above 20 ms. Secondly, the

countereffect of high spacing factors introduces numerical instability into the calculation of the speckle contrast. Falsely observed high contrast values increase the cost; numerical instability appears at smaller spacing factors for shorter exposure times. Subplots b) showcase the intensity penalized cost surface. The significant difference between the raw and the penalized versions is that the cost towards the larger spacing factors is affected by an additional term, which penalizes the underexposed images in a linear way. The start of the penalization – when the exposure falls below the predefined threshold – is dependent on the actual exposure length as expected.

The theoretical minimum moves toward the continuous wave operation mode for larger values, as it is indicated by the black circle on the envelope. Such behavior is expected since larger spacing factors have a great effect on the dynamic range, making the response so wide that the contrast values fall below the reference values, hence increasing the cost. Fig. 10 depicts the Pareto front around the minimum; it can be seen that similar costs are achieved with different combinations of exposure length and spacing factor.
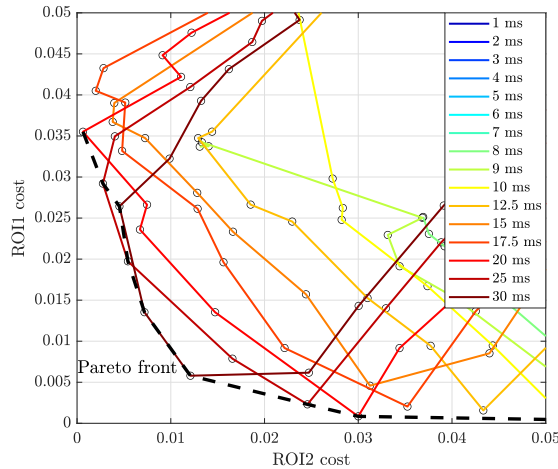

Figure 10

As the dynamic range maximization in (6) is formulated as a multi-objective optimization, a Pareto front can be found, where ROI1 and ROI2 costs represent the distances from the reference contrast value.

Conclusions

In this study, we proposed the sample-in-the-loop approach for LSCI applications. We defined three use cases in order to demonstrate the applicability of the method. We did not aim to prove or validate the utilization of the three use cases but to demonstrate the concept through different scenarios.

In the first scenario, the algorithm realized a setpoint optimization for the

reference contrast value and was able to compensate for an external disturbance coming from flow speed change. The solution can be a help running automated measurements, however, it is important to note that the method can provide information only about the relative flow speeds in a given time instant or if the external factors are constant. This is the case since the algorithm will compensate (in a feasible range) for changes in external factors such as flow speed.

Previous studies indicated and our findings confirmed that the sensitivity maximization is best achieved as a continuous wave operation, where we optimized the exposure length using the gradient descent algorithm. Regarding the dynamic range maximization, we demonstrated that the proposed algorithm can find a minimum, and this minimum is dependent on the actual reference contrast value. Furthermore, with the current laser setup, the exposure penalization leaves small room for dynamic range improvements. This highlights the importance of sufficiently high laser power as large spacing factors reduced the total exposure by more than an order of magnitude. The explored cost surface indicates that it is sufficient to use gradient descent in the multivariate case as well since the cost surface is a convex function with respect to the free variables. The application of the gradient descent can then accelerate the convergence to a minimum and the fulfillment of the measurement protocol.

Acknowledgement

References

[1] R. Smith-Bindman, M. L. Kwan, E. C. Marlow, M. K. Theis, W. Bolch, S. Y. Cheng, E. J. A. Bowles, J. R. Duncan, R. T. Greenlee, L. H. Kushi, J. D. Pole, A. K. Rahm, N. K. Stout, S. Weinmann, and D. L. Miglioretti. Trends in Use of Medical Imaging in US Health Care Systems and in Ontario, Canada, 2000-2016. *JAMA*, 322(9):843–856, 09 2019.

[2] W. Heeman, W. Steenbergen, G. M. van Dam, and E. C. Boerma. Clinical applications of laser speckle contrast imaging: a review. *Journal of Biomedical Optics*, 24(8):1 – 11, 2019.

[3] D. Briers, D. Duncan, E. Hirst, S. Kirkpatrick, M. Larsson, W. Steenbergen, T. Stromberg, and O. Thompson. Laser speckle contrast imaging: Theoretical and practical limitations. *Journal of biomedical optics*, 18:66018, 06 2013.

[4] C. Wang, Z. Cao, X. Jin, W. Lin, Y. Zheng, B. Zeng, and M. Xu. Robust quantitative single-exposure laser speckle imaging with true flow speckle contrast in the temporal and spatial domains. *Biomed. Opt. Express*, 10(8):4097–4114, Aug 2019.

[5] P. Földesy, M. Siket, I. Jánoki, K. Demeter, and Ádám Nagy. Ensemble averaging laser speckle contrast imaging: statistical model of improvement as function of static scatterers. *Opt. Express*, 29(18):29366–29377, Aug

2021.

[6] A. Fercher and J. Briers. Flow visualization by means of single-exposure speckle photography. *Optics Communications*, 37(5):326–330, 1981.

[7] O. A. Mennes, J. J. van Netten, J. G. van Baal, and W. Steenbergen. Assessment of microcirculation in the diabetic foot with laser speckle contrast imaging. 40(6):065002, jul 2019.

[8] B. S. Lertsakdadet, G. T. Kennedy, R. Stone, C. Kowalczewski, A. C. Kowalczewski, S. Natesan, R. J. Christy, A. J. Durkin, and B. Choi. Assessing multimodal optical imaging of perfusion in burn wounds. *Burns*, 2021.

[9] K. Zheng, E. Middelkoop, M. Stoop, P. van Zuijlen, and A. Pijpe. Validity of laser speckle contrast imaging for the prediction of burn wound healing potential. *Burns*, 48(2):319–327, 2022.

[10] G. J. Richards and J. D. Briers. Capillary-blood-flow monitoring using laser speckle contrast analysis (LASCA): improving the dynamic range. In V. V. Tuchin, H. P. M.D., and B. Ovryn, editors, *Coherence Domain Optical Methods in Biomedical Science and Clinical Applications*, volume 2981, pages 160 – 171. International Society for Optics and Photonics, SPIE, 1997.

[11] A. B. Parthasarathy, W. J. Tom, A. Gopal, X. Zhang, and A. K. Dunn. Robust flow measurement with multi-exposure speckle imaging. *Optics Express*, 16(3):1975–1989, 2008.

[12] T. Dragojević, D. Bronzi, H. M. Varma, C. P. Valdes, C. Castellvi, F. Villa, A. Tosi, C. Justicia, F. Zappa, and T. Durduran. High-speed multi-exposure laser speckle contrast imaging with a single-photon counting camera. *Biomedical Optics Express*, 6(8):2865–2876, 2015.

[13] L. Song and D. S. Elson. Effect of signal intensity and camera quantization on laser speckle contrast analysis. *Biomed. Opt. Express*, 4(1):89–104, Jan 2013.

[14] S. Sunil, S. Zilpelwar, D. A. Boas, and D. D. Postnov. Guidelines for obtaining an absolute blood flow index with laser speckle contrast imaging. *bioRxiv*, 2021.

[15] M. Siket, I. Jánoki, K. Demeter, M. Szabó, and P. Földesy. Time varied illumination laser speckle contrast imaging. *Opt. Lett.*, 46(4):713–716, Feb 2021.

[16] M. Hultman, M. Larsson, T. Strömberg, and I. Fredriksson. Real-time video-rate perfusion imaging using multi-exposure laser speckle contrast imaging and machine learning. *Journal of Biomedical Optics*, 25(11):116007, 2020.

[17] P. Földesy, M. Siket, Ádám Nagy, and I. Jánoki. Correction of overexposure in laser speckle contrast imaging. *Opt. Express*, 30(12):21523–21534, Jun 2022.

[18] C. Wang, Z. Cao, X. Jin, W. Lin, Y. Zheng, B. Zeng, and M. Xu. Robust quantitative single-exposure laser speckle imaging with true flow speckle contrast in the temporal and spatial domains. *Biomed. Opt. Express*, 10(8):4097–4114, Aug 2019.

[19] M. Ikeda. Switching characteristics of laser diode switch. *IEEE Journal of Quantum Electronics*, 19(2):157–164, 1983.

[20] C. Inc. Comsol, 2020. http://www.comsol.com/products/multiphysics/.

[21] Y. Zhao, K. Wang, W. Li, H. Zhang, Z. Qian, and Y. Liu. Laser speckle contrast imaging system using nanosecond pulse laser source. *Journal of Biomedical Optics*, 25(05):1–10, 2020.

[22] O. Thompson, M. Andrews, and E. Hirst. Correction for spatial averaging in laser speckle contrast analysis. *Biomed. Opt. Express*, 2(4):1021–1029, Apr 2011.

[23] H. Khan and J. K. Tar. On the Implementation of Fixed Point Iteration-based Adaptive Receding Horizon Control for Multiple Degree of Freedom, Higher Order Dynamical Systems. *Acta Polytechnica Hungarica*, 16(9):20, 2019.

[24] A. J. Babqi and B. Alamri. A Comprehensive Comparison between Finite Control Set Model Predictive Control and Classical Proportional-Integral Control for Grid-tied Power Electronics Devices. *Acta Polytechnica Hungarica*, 18(7):67–87, 2021.

[25] R.-C. Roman, R.-E. Precup, E.-L. Hedrea, S. Preitl, I. A. Zamfirache, C.-A. Bojan-Dragos, and E. M. Petriu. Iterative Feedback Tuning Algorithm for Tower Crane Systems. *Procedia Computer Science*, 199:157–165, 2022.

[26] H. Redjimi and J. K. Tar. Multiple Components Fixed Point Iteration in the Adaptive Control of Single Variable 2nd Order Systems. *Acta Polytechnica Hungarica*, 18(9):69–86, 2021.

[27] S. G. Johnson. The nlopt nonlinear-optimization package. https://github.com/stevengj/nlopt.